

BK-SDM: A Lightweight, Fast, and Cheap Version of Stable Diffusion

Bo-Kyeong Kim¹ Hyoung-Kyu Song¹ Thibault Castells¹ Shinkook Choi¹
¹Nota Inc.

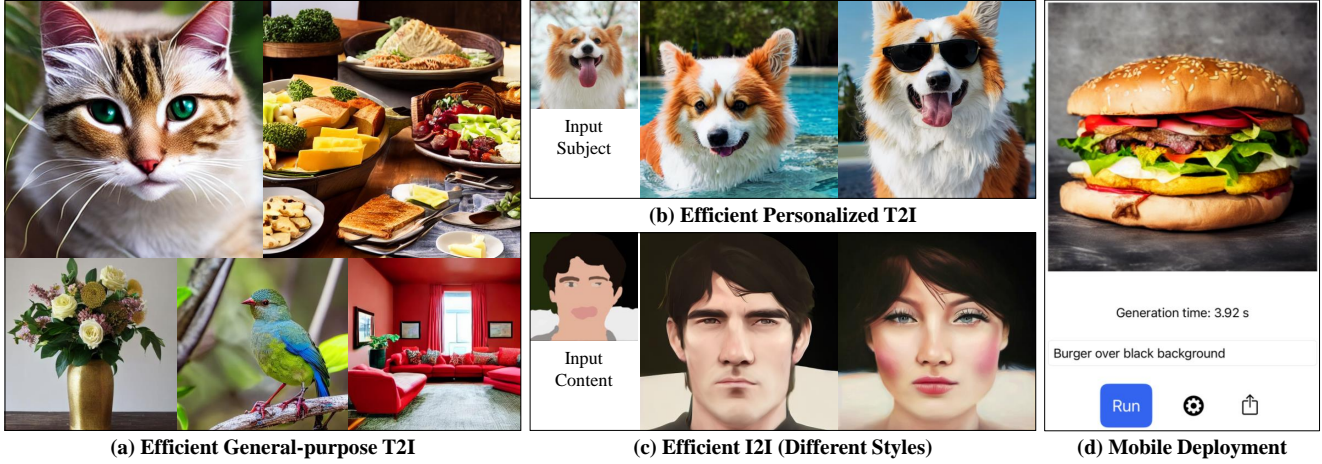


Figure 1. Our compressed Stable Diffusion enables efficient (a) zero-shot text-to-image generation, (b) personalized synthesis, (c) image-to-image translation, and (d) mobile deployment. Samples from BK-SDM-Small with 36% reduced parameters and latency are shown.

Abstract

Text-to-image (T2I) generation with Stable Diffusion models (SDMs) involves high computing demands due to billion-scale parameters. To enhance efficiency, recent studies have reduced sampling steps and applied network quantization while retaining the original architectures. The lack of architectural reduction attempts may stem from worries over expensive retraining for such massive models. In this work, we uncover the surprising potential of block pruning and feature distillation for low-cost general-purpose T2I. By removing several residual and attention blocks from the U-Net of SDMs, we achieve 30%~50% reduction in model size, MACs, and latency. We show that distillation retraining is effective even under limited resources: using only 13 A100 days and a tiny dataset, our compact models can imitate the original SDMs (v1.4 and v2.1-base with over 6,000 A100 days). Benefiting from the transferred knowledge, our BK-SDMs deliver competitive results on zero-shot MS-COCO against larger multi-billion parameter models. We further demonstrate the applicability of our lightweight backbones in personalized generation and image-to-image translation. Deployment of our models on edge devices attains 4-second inference. We hope this work can help build small yet power-

ful diffusion models with feasible training budgets.

1. Introduction

Stable Diffusion models (SDMs) [52, 55] are one of the most renowned open-source models for text-to-image (T2I) synthesis, and their exceptional capability has begun to be leveraged as a backbone in several text-guided vision applications [2, 3, 78, 81]. SDMs are T2I-specialized latent diffusion models (LDMs) [55], which employ diffusion operations [20, 33, 70] in a semantically compressed space for compute efficiency. Within a SDM, a U-Net [7, 58] performs iterative sampling to progressively denoise a random latent code and is aided by a text encoder [48] and an image decoder [10, 75] to produce text-aligned images. This inference process still involves excessive computational requirements (see Fig. 2), which often hinder the utilization of SDMs despite their rapidly growing usage.

To alleviate this issue, numerous approaches toward efficient SDMs have been introduced. A pretrained diffusion model is distilled to reduce the number of denoising steps, enabling an identically architected model with fewer sampling steps [37, 39]. Post-training quantization [22, 30, 68] and implementation optimization [5] methods are also leveraged. However, the removal of architectural elements in

large diffusion models remains less explored.

This study unlocks the immense potential of classical architectural compression in attaining smaller and faster diffusion models. We eliminate multiple residual and attention blocks from the U-Net of a SDM and retrain it with feature-level knowledge distillation (KD) [16, 57] for general-purpose T2I. Under restricted training resources, our compact models can mimic the original SDM by leveraging transferred knowledge. Our work effectively reduces the computation of SDM-v1.4 [52] and SDM-v2.1-base [56] while achieving compelling zero-shot results on par with multi-billion parameter models [8, 9, 49]. Our contributions are summarized as follows:

- We compress SDMs by removing architectural blocks from the U-Net, achieving up to 51% reduction in model size and 43% improvement in latency on CPU and GPU. Previous pruning studies [11, 41, 79] focused on small models ($<100\text{M}$ parameters) like ResNet50 and DeiT-B, not on foundation models like SDMs ($>1,000\text{M}=1\text{B}$), possibly due to the lack of economic retraining for such large models. Moreover, U-Net architectures are arguably more complex due to the necessity of considering skip connections across the network, making the structural block removal inside them not straightforward.
- To the best of our knowledge, we first demonstrate the notable benefit of feature distillation for training diffusion models, which enables competitive T2I even with significantly fewer resources (using only 13 A100 days and 0.22M LAION pairs [64]). Considering the vast expense of training SDMs from scratch (surpassing 6,000 A100 days and 2,000M pairs), our study indicates that network compression is a remarkably cost-effective strategy in building compact general-purpose diffusion models.
- We show the practicality of our work across various aspects. Our lightweight backbones are readily applicable to customized generation [59] and image-to-image translation [38], effectively lowering finetuning and inference costs. T2I synthesis on Jetson AGX Orin and iPhone 14 using our models takes less than 4 seconds.
- We have publicly released our approach, model weights, and source code: <https://github.com/Nota-NetsPresso/BK-SDM>. Interesting subsequent works include block pruning and KD for the SDM-v1 variant [66] and SDXL [67].

2. Related work

Large T2I diffusion models. By gradually removing noise from corrupted data, diffusion-based generative models [7, 21, 70] enable high-fidelity synthesis with broad mode coverage. Integrating these merits with the advancement of pretrained language models [6, 47, 48] has significantly improved the quality of T2I synthesis. In GLIDE [42] and Imagen [60], a text-conditional diffusion model generates a

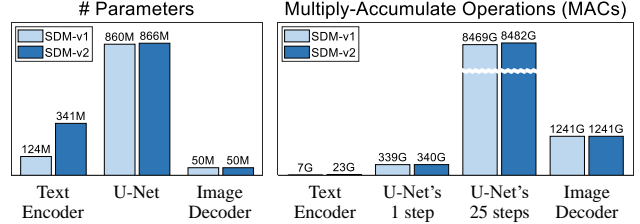


Figure 2. **Computation of Stable Diffusion v1 and v2.** The denoising U-Net is the main processing bottleneck. THOP [85] is used to measure MACs in generating a 512×512 image.

small image, which is upsampled via super-resolution modules. In DALL-E-2 [50], a text-conditional prior network produces an image embedding, which is transformed into an image via a diffusion decoder and further upsampled into higher resolutions. SDMs [52, 53, 55, 56] perform the diffusion modeling in a low-dimensional latent space constructed through a pixel-space autoencoder. We use SDMs as our baseline because of its open-access and gaining popularity over numerous downstream tasks [2, 3, 59, 78].

Efficient diffusion models. Several studies have addressed the slow sampling process. Diffusion-tailored distillation [37, 39, 61] progressively transfers knowledge from a pretrained diffusion model to a fewer-step model with the same architecture. Fast high-order solvers [34, 35, 83] for diffusion ordinary differential equations boost the sampling speed. Complementarily, our network compression approach reduces per-step computation and can be easily integrated with less sampling steps. Leveraging quantization [22, 30, 68] and implementation optimizations [5] for SDMs can also be combined with our compact models for further efficiency.

Distillation-based compression. KD enhances the performance of small-size models by exploiting output-level [19, 44] and feature-level [16, 57, 80] information of large source models. Although this classical KD has been actively used for efficient GANs [29, 51, 82], its power has not been explored for structurally compressed diffusion models. Distillation pretraining enables small yet capable general-purpose language models [24, 63, 71] and vision transformers [14, 74]. Beyond such models, we show that its success can be extended to diffusion models with iterative sampling.

Concurrent studies. SnapFusion [31] achieves an efficient U-Net for SDMs through architecture evolution and step distillation. Würstchen [45] introduces two diffusion processes on low- and high-resolution latent spaces for economic training. These two works are valuable but require much larger resources than our work (see Tab. 1). While not demonstrated on SDMs, Diff-Pruning [12] proposes structured pruning based on Taylor expansion tailored for diffusion models.

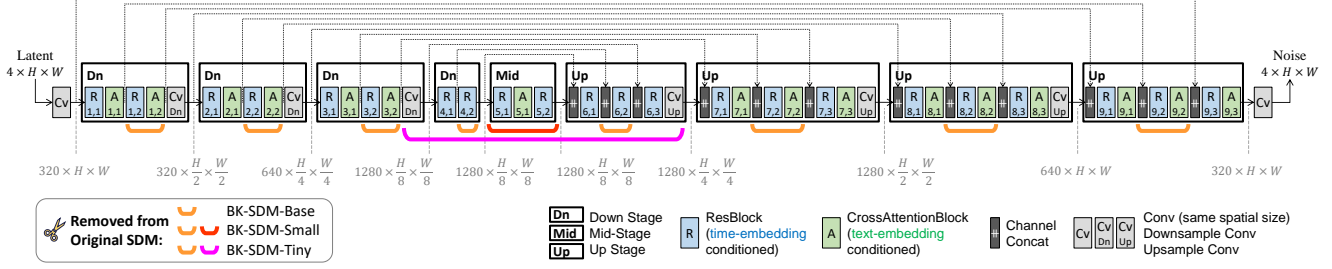


Figure 3. **Block removal from the denoising U-Net.** Our approach is applicable to all the SDM versions in v1 and v2, which share the same U-Net block configuration. For experiments, we used v1.4 [52] and v2.1-base [56]. See Sec. A for the detailed architectures.



Figure 4. **Minor impact of removing the mid-stage from the U-Net.** Results without retraining. See Sec. B for additional results.

3. Compression Method

We compress the U-Net [58] in SDMs, which is the most compute-heavy component (see Fig. 2). Conditioned on the text and time-step embeddings, the U-Net performs multiple denoising steps on latent representations. At each step, the U-Net produces the noise residual to compute the latent for the next step. We reduce this per-step computation, leading to *Block-removed Knowledge-distilled SDMs* (BK-SDMs).

3.1. Compact U-Net architecture

The following architectures are obtained by compressing SDM-v1 (1.04B parameters), as shown in Fig. 3:

- BK-SDM-Base (0.76B) obtained with Sec. 3.1.1.
- BK-SDM-Small (0.66B) with Secs. 3.1.1 and 3.1.2.
- BK-SDM-Tiny (0.50B) with Secs. 3.1.1, 3.1.2, and 3.1.3.

Our approach can be identically applied to SDM-v2 (1.26B parameters), leading to BK-SDM-v2-{Base (0.98B), Small (0.88B), Tiny (0.72B)}.

3.1.1 Fewer blocks in the down and up stages

This approach is closely aligned with DistilBERT [63] which halves the number of layers and initializes the compact model with the original weights by benefiting from the shared dimensionality. In the original U-Net, each stage with a common spatial size consists of multiple blocks, and most stages contain pairs of residual (R) [15] and cross-attention (A) [23, 76] blocks. We hypothesize the existence of some unnecessary pairs and use the following removal strategies.

Down stages. We maintain the first R-A pairs while eliminating the second pairs, because the first pairs process the

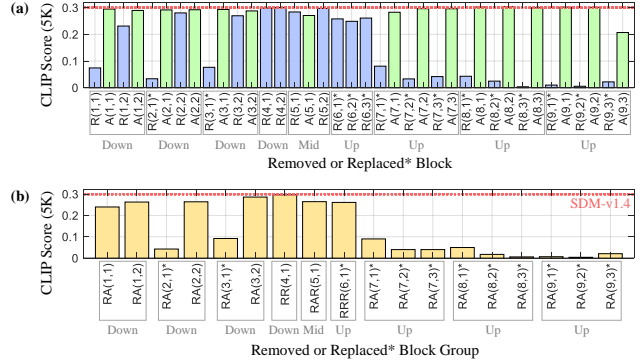


Figure 5. **Importance of (a) each block and (b) each group of paired/triplet blocks.** Higher score implies removable blocks. The results are aligned with our architectures (e.g., removal of innermost stages and the second R-A pairs in down stages). See Sec. C for further analysis.

changed spatial information and would be more important than the second pairs. This design is consistent with the pruning sensitivity analysis that measures the block-level significance (see Fig. 5). Our approach also does not harm the dimensionality of the original U-Net, enabling the use of the corresponding pretrained weights for initialization [63].

Up stages. While adhering to the aforementioned scheme, we retain the third R-A pairs. This allows us to utilize the output feature maps at the end of each down stage and the corresponding skip connections between the down and up stages. The same process is applied to the innermost down and up stages that contain only R blocks.

3.1.2 Removal of the entire mid-stage

Surprisingly, removing the entire mid-stage from the original U-Net does not noticeably degrade the generation quality while effectively reducing the parameters by 11% (see Fig. 4). This observation is consistent with the minor role of inner layers in the U-Net generator of GANs [27].

Integrating the mid-stage removal with fewer blocks in Sec. 3.1.1 further decreases compute burdens (Tab. 2) at the

cost of a slight decline in performance (Tab. 1). Therefore, we offer this mid-stage elimination as an option, depending on the priority between compute efficiency (using BK-SDM-Small) and generation quality (BK-SDM-Base).

3.1.3 Further removal of the innermost stages

For additional compression, the innermost down and up stages can also be pruned, leading to our lightest model BK-SDM-Tiny. This implies that outer stages with larger spatial dimensions and their skip connections play a crucial role in the U-Net for T2I synthesis.

3.1.4 Alignment with pruning sensitivity analysis

To support the properness of our architectures, we measure the importance of each block (see Fig. 5) and show that unimportant blocks match with our design choices. The importance is measured by how generation scores vary when removing each residual or attention block from the U-Net. A significant drop in performance highlights the essential role of that block. Note that some blocks are not directly removable due to different channel dimensions between input and output; we replace such blocks with channel interpolation modules (denoted by “*” in Fig. 5) to mimic the removal while retaining the information.

The sensitivity analysis implies that the innermost down-mid-up stages and the second R-A pairs in the down stages play relatively minor roles. Pruning these blocks aligns with our architectures, designed based on human knowledge (e.g., prioritizing blocks with altered channel dimensions) and previous studies [27, 63].

3.2. Distillation-based retraining

For general-purpose T2I, we train our block-removed U-Net to mimic the behavior of the original U-Net (see Fig. 6). To obtain the input of U-Net, we use pretrained-and-frozen encoders [55] for images and text prompts.

Given the latent representation \mathbf{z} of an image and its paired text embedding \mathbf{y} , the task loss for the reverse denoising process [21, 55] is computed as:

$$\mathcal{L}_{\text{Task}} = \mathbb{E}_{\mathbf{z}, \epsilon, \mathbf{y}, t} \left[\|\epsilon - \epsilon_S(\mathbf{z}_t, \mathbf{y}, t)\|_2^2 \right], \quad (1)$$

where \mathbf{z}_t is a noisy latent code from the diffusion process [21] with the sampled noise $\epsilon \sim N(\mathbf{0}, \mathbf{I})$ and time step $t \sim \text{Uniform}(1, T)$, and $\epsilon_S(\circ)$ indicates the estimated noise from our compact U-Net student. For brevity, we omit the subscripts of $\mathbb{E}_{\mathbf{z}, \epsilon, \mathbf{y}, t}[\circ]$ in the following notations.

The compact student is also trained to imitate the outputs of the original U-Net teacher, $\epsilon_T(\circ)$, with the following output-level KD objective [19]:

$$\mathcal{L}_{\text{OutKD}} = \mathbb{E} \left[\|\epsilon_T(\mathbf{z}_t, \mathbf{y}, t) - \epsilon_S(\mathbf{z}_t, \mathbf{y}, t)\|_2^2 \right]. \quad (2)$$

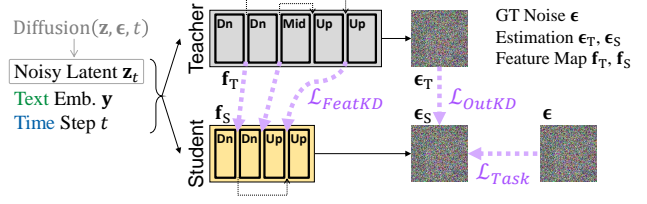


Figure 6. **Distillation-based retraining.** The block-removed U-Net is trained effectively through the guidance of the original U-Net.

A key to our approach is feature-level KD [16, 57] that provides abundant guidance for the student’s training:

$$\mathcal{L}_{\text{FeatKD}} = \mathbb{E} \left[\sum_l \|f_T^l(\mathbf{z}_t, \mathbf{y}, t) - f_S^l(\mathbf{z}_t, \mathbf{y}, t)\|_2^2 \right], \quad (3)$$

where $f_T^l(\circ)$ and $f_S^l(\circ)$ represent the feature maps of the l -th layer in a predefined set of distilled layers from the teacher and the student, respectively. While learnable regressors (e.g., 1×1 convolutions to match the number of channels) have been commonly used [51, 57, 69], our approach circumvents this requirement. By applying distillation at the end of each stage in both models, we ensure that the dimensionality of the feature maps already matches, thus eliminating the need for additional regressors.

The final objective is shown below, and we simply set λ_{OutKD} and λ_{FeatKD} as 1. Without loss-weight tuning, our approach is effective in empirical validation.

$$\mathcal{L} = \mathcal{L}_{\text{Task}} + \lambda_{\text{OutKD}} \mathcal{L}_{\text{OutKD}} + \lambda_{\text{FeatKD}} \mathcal{L}_{\text{FeatKD}}. \quad (4)$$

4. Experimental setup

Distillation retraining. We primarily use 0.22M image-text pairs from LAION-Aesthetics V2 (L-Aes) 6.5+ [64, 65], which are significantly fewer than the original training data used for SDMs [52, 56] (>2,000M pairs). In Fig. 11, dataset sizes smaller than 0.22M are randomly sampled from L-Aes 6.5+, while those larger than 0.22M are from L-Aes 6.25+.

Zero-shot T2I evaluation. Following the popular protocol [49, 55, 60], we use 30K prompts from the MS-COCO validation split [32], downsample the 512×512 generated images to 256×256 , and compare them with the entire validation set. We compute Fréchet Inception Distance (FID) [18] and Inception Score (IS) [62] to assess visual quality. We measure CLIP score [17, 48] with CLIP-ViT-g/14 model to assess text-image correspondence.

Downstream tasks. For personalized generation, we use the DreamBooth dataset [59] (30 subjects \times 25 prompts \times 4~6 images) and perform per-subject finetuning. Following the evaluation protocol [59], we use ViT-S/16 model [4] for DINO score and CLIP-ViT-g/14 model for CLIP-I and CLIP-T scores. For image-to-image translation, input images are sourced from Meng *et al.* [39].

Model			Generation Score			Training Resource		
Name	Type	# Param [‡]	FID↓	IS↑	CLIP↑	Data Size	(Batch, # Iter)	A100 Days
SDM-v1.4 [52, 55] [†]	DF	1.04B	13.05	36.76	0.2958	>2000M*	(2048, 1171K)	6250
Small Stable Diffusion [46] [†]	DF	0.76B	12.76	32.33	0.2851	229M	(128, 1100K)	-
BK-SDM-Base [Ours] [†]	DF	0.76B	15.76	33.79	0.2878	0.22M	(256, 50K)	13
BK-SDM-Small [Ours] [†]	DF	0.66B	16.98	31.68	0.2677	0.22M	(256, 50K)	13
BK-SDM-Tiny [Ours] [†]	DF	0.50B	17.12	30.09	0.2653	0.22M	(256, 50K)	13
SDM-v2.1-base [55, 56] [†]	DF	1.26B	13.93	35.93	0.3075	>2000M*	(2048, 1620K)	8334
BK-SDM-v2-Base [Ours] [†]	DF	0.98B	15.85	31.70	0.2868	0.22M	(128, 50K)	4
BK-SDM-v2-Small [Ours] [†]	DF	0.88B	16.61	31.73	0.2901	0.22M	(128, 50K)	4
BK-SDM-v2-Tiny [Ours] [†]	DF	0.72B	15.68	31.64	0.2897	0.22M	(128, 50K)	4
DALL-E [49]	AR	12B	27.5	17.9	-	250M	(1024, 430K)	-
CogView [8]	AR	4B	27.1	18.2	-	30M	(6144, 144K)	-
CogView2 [9]	AR	6B	24	22.4	-	30M	(4096, 300K)	-
Make-A-Scene [13]	AR	4B	11.84	-	-	35M	(1024, 170K)	-
LAFITE [84]	GAN	0.23B	26.94	26.02	-	3M	-	-
GALIP (CC12M) [73] [†]	GAN	0.32B	13.86	25.16	0.2817	12M	-	-
GigaGAN [25]	GAN	1.1B	9.09	-	-	>100M*	(512, 1350K)	4783
GLIDE [42]	DF	3.5B	12.24	-	-	250M	(2048, 2500K)	-
LDM-KL-8-G [55]	DF	1.45B	12.63	30.29	-	400M	(680, 390K)	-
DALL-E-2 [50]	DF	5.2B	10.39	-	-	250M	(4096, 3400K)	-
SnapFusion [31]	DF	0.99B	~13.6	-	~0.295	>100M*	(2048, -)	>128*
Würstchen-v2 [45] [†]	DF	3.1B	22.40	32.87	0.2676	1700M	(1536, 1725K)	1484

[†]: Evaluated with the released checkpoints. [‡]: Total parameters for T2I synthesis. *: Estimated based on public information.
DF and AR: diffusion and autoregressive models. ↓ and ↑: lower and higher values are better.

Table 1. **Results on zero-shot MS-COCO 256×256 30K.** Training resources include image-text pairs, batch size, iterations, and A100 days. Despite far smaller resources, our compact models outperform prior studies [8, 9, 49, 73, 84], showing the benefit of compressing existing powerful models. Note that FID fluctuates more than the other metrics over training progress in our experiments (see Figs. 9 and 11).

Implementation details. We adjust the codes in Diffusers [77] and PEFT [36]. We use a single NVIDIA A100 80G GPU for main retraining and a single NVIDIA GeForce RTX 3090 GPU for per-subject finetuning. For compute efficiency, we always opt for 25 denoising steps of the U-Net at the inference phase, unless specified. The classifier-free guidance scale [20, 60] is set to the default value of 7.5. The latent resolution is set to the default ($H = W = 64$ in Fig. 3), yielding 512×512 images. See Sec. I for the details.

5. Results

All the results in Secs. 5.1–5.4 were obtained with the full benchmark protocol (MS-COCO 256×256 30K samples), except for Fig. 10 (512×512 5K samples). Unless specified, the training setup in Tab. 1 was used.

5.1. Comparison with existing works

Quantitative comparison. Tab. 1 shows the zero-shot results for general-purpose T2I. Despite being trained with only 0.22M samples and having fewer than 1B parameters, our compressed models demonstrate competitive performance on par with existing large models. A recent small SDM without paper evidence [46] relies on far more training resources: two-stage KD with two teachers (SDM-v1.4 and

v1.5) and significantly longer iterations on a much larger dataset. In contrast, our lighter models yield compelling results while saving on training budgets.

Visual comparison. Fig. 7 depicts synthesized images with some MS-COCO captions. Our compact models inherit the superiority of SDM and produce more photorealistic images compared to the AR-based [9] and GAN-based [73, 84] baselines. Noticeably, the same latent code results in a shared visual style between the original and our models (6th–9th columns in Fig. 7), similar to the observation in transfer learning for GANs [40]. See Sec. D for additional results.

5.2. Computational gain

Tab. 2 shows how the compute reduction for each sampling step of the U-Net affects the overall process. The per-step reduction effectively decreases MACs and inference time by more than 30%. Notably, BK-SDM-Tiny has 50% fewer parameters than the original SDM.

5.3. Benefit of distillation retraining

T2I performance. Tab. 3 summarizes the results from ablating the total KD objective (Eq. 2+Eq. 3). Across various model types, distillation brings a clear improvement in generation quality. Tab. 4 analyzes the effect of each element in



Prompt: A bowl that has vegetables inside of it.; A brown and white cat staring off with pretty green eyes.; A toy raccoon standing on a pile of broccoli.

Figure 7. **Visual comparison with open-sourced models.** The results [9, 42, 45, 73, 84] were obtained with their official codes.

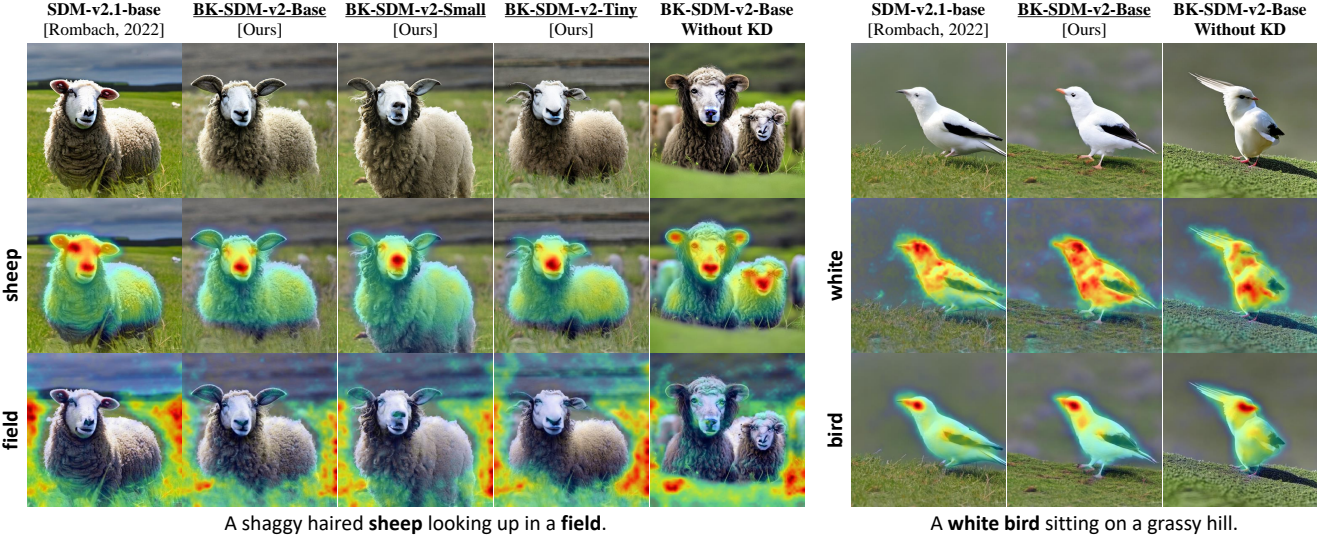


Figure 8. **Image areas affected by each word.** KD enables our models to mimic the SDM, yielding similar per-word attribution maps. The model without KD behaves differently, causing dissimilar maps and inaccurate generation (e.g., two sheep and unusual bird shapes).

transferred knowledge. Exploiting output-level KD (Eq. 2) boosts the performance compared to using only the denoising task loss. Leveraging feature-level KD (Eq. 3) yields further score enhancement. Additionally, using the teacher weights for initialization is highly beneficial.

Cross-attention resemblance. Fig. 8 displays the per-word attribution maps [72] created by aggregating cross-attention scores over spatiotemporal dimensions. The attribution maps of our models are semantically and spatially similar to those of the original model, indicating the merit of supervisory signals at multiple stages via KD. In contrast, the baseline model without KD activates incorrect areas, leading to text-mismatched generation results.

Training progress. Fig. 9 shows the results over training iterations. Without KD, training solely with the denoising task loss causes fluctuations or sudden drops in performance (indicated with green and cyan). In contrast, distillation (purple and pink) stabilizes and accelerates the training process, demonstrating the benefit of providing sufficient hints for training guidance. Notably, our small- and tiny-size models trained with KD (yellow and red) outperform the bigger base-size model without KD (cyan). Additionally, while the best FID score is observed early on, IS and CLIP score exhibit ongoing improvement, implying that judging models merely with FID may be suboptimal.

Trade-off results. Fig. 10 shows the results of BK-SDM-

Model	# Param		MACs			CPU Latency			GPU Latency		
	U-Net	Whole	U-Net (1)	U-Net (25)	Whole	U-Net (1)	U-Net (25)	Whole	U-Net (1)	U-Net (25)	Whole
SDM-v1.4 [52]	860M	1033M	339G	8469G	9716G	5.63s	146.28s	153.00s	0.049s	1.28s	1.41s
BK-SDM-Base [Ours]	580M	752M	224G	5594G	6841G	3.84s	99.95s	106.67s	0.032s	0.83s	0.96s
	(-32.6%)	(-27.1%)	(-33.9%)	(-33.9%)	(-29.5%)	(-31.8%)	(-31.7%)	(-30.3%)	(-34.6%)	(-35.2%)	(-31.9%)
BK-SDM-Small [Ours]	483M	655M	218G	5444G	6690G	3.45s	89.78s	96.50s	0.030s	0.77s	0.90s
	(-43.9%)	(-36.5%)	(-35.7%)	(-35.7%)	(-31.1%)	(-38.7%)	(-38.6%)	(-36.9%)	(-38.7%)	(-39.8%)	(-36.1%)
BK-SDM-Tiny [Ours]	324M	496M	206G	5126G	6373G	3.03s	78.77s	85.49s	0.026s	0.67s	0.80s
	(-62.4%)	(-51.9%)	(-39.5%)	(-39.5%)	(-34.4%)	(-46.2%)	(-46.1%)	(-44.1%)	(-46.9%)	(-47.7%)	(-43.2%)

Table 2. **Impact of compute reduction in U-Net on the entire SDM.** The number of sampling steps is indicated with the parentheses, e.g., U-Net (1) for one step. The full computation (denoted by “Whole”) covers the text encoder, U-Net, and image decoder. All corresponding values are obtained on the generation of a single 512×512 image with 25 denoising steps. The latency was measured on Xeon Silver 4210R CPU 2.40GHz and NVIDIA GeForce RTX 3090 GPU.

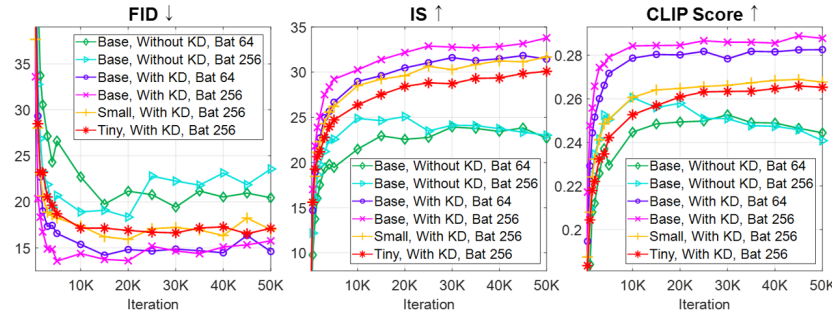


Figure 9. **Zero-shot results over training progress.** The architecture size of BK-SDM, usage of KD, and batch size are denoted. Results on MS-COCO 30K.

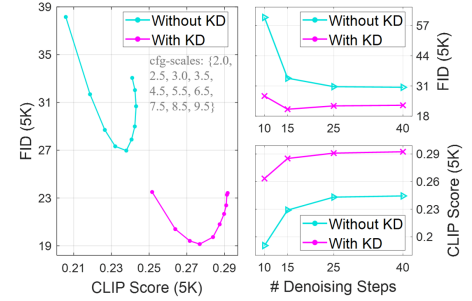


Figure 10. **Trade-off curves.** Left: FID vs. CLIP score; Right: generation quality vs. efficiency. BK-SDM-Base on MS-COCO 5K.

BK-SDM		Generation Score			# Param	
Type	KD	FID↓	IS↑	CLIP↑	U-Net	Whole
Base	✗	23.57	23.02	0.2408	0.58B	0.76B
	✓	15.76	33.79	0.2878	0.58B	0.76B
v2-Base	✗	16.76	25.88	0.2661	0.59B	0.98B
	✓	15.85	31.70	0.2868	0.59B	0.98B
v2-Small	✗	16.71	25.77	0.2655	0.49B	0.88B
	✓	16.61	31.73	0.2901	0.49B	0.88B
v2-Tiny	✗	16.87	26.06	0.2678	0.33B	0.72B
	✓	15.68	31.64	0.2897	0.33B	0.72B

Table 3. **Performance gains from distillation retraining.** Results on MS-COCO 30K.

BK-SDM	Init	OutKD	FeatKD	FID↓	IS↑	CLIP↑
Base (Batch 64)	Random	✗	✗	43.80	13.61	0.1622
	Teacher	✗	✗	20.45	22.68	0.2444
	Teacher	✓	✗	16.48	27.30	0.2620
	Teacher	✓	✓	14.61	31.44	0.2826
v2-Small	Random	✗	✗	41.75	15.42	0.1733
	Teacher	✗	✗	16.71	25.77	0.2655
	Teacher	✓	✗	14.27	29.47	0.2777
	Teacher	✓	✓	16.61	31.73	0.2901

Init: weight initialization. (OutKD, FeatKD): (output, feature)-level KD.

Table 4. **Significance of each element in transferred knowledge.** Results on MS-COCO 30K.

Base with and without KD on MS-COCO 512×512 5K. Higher classifier-free guidance scales [20, 60] lead to better text-aligned images at the cost of less diversity. More denoising steps improve generation quality at the cost of slower inference. Distillation retraining achieves much better trade-off curves than the baseline without KD.

5.4. Impact of training resources on performance

Consistent with existing evidence, the use of larger batch sizes, more extensive data, and longer iterations for training enhances performance in our work (see Tab. 5, Fig. 11, and Sec. H). However, this benefit requires increased resource demands (e.g., extended training days without multiple high-spec GPUs and greater data storage capacity). As such, despite the better performing models in Tab. 5, we primarily report the models with fewer resources. We believe that accessible training costs by many researchers can help drive advancement in massive models.

5.5. Application

Personalized T2I synthesis. Tab. 6 compares the fine-tuning results with DreamBooth [59] over different backbones to create images about a given subject. BK-SDMs can preserve 95%~99% scores of the original SDM while cutting fine-tuning costs. Fig. 12 depicts that our models can accurately capture the subject details and generate various scenes. Over

BK-SDM	Base		Small		Tiny	
Batch Size	64	256	64	256	64	256
FID↓	14.61	15.76	16.87	16.98	17.28	17.12
IS↑	31.44	33.79	29.51	31.68	28.33	30.09
CLIP↑	0.2826	0.2878	0.2644	0.2677	0.2607	0.2653

BK-SDM	Base (Data 2.3M)		Small (Data 2.3M)		Tiny (Data 2.3M)	
# Iter	50K	100K	50K	100K	50K	100K
FID↓	14.81	15.39	17.05	17.01	17.53	17.63
IS↑	34.17	34.76	33.10	33.14	31.32	32.26
CLIP↑	0.2883	0.2889	0.2734	0.2754	0.2690	0.2713

Table 5. **Impact of training batch size and iterations.** Results on MS-COCO 30K.

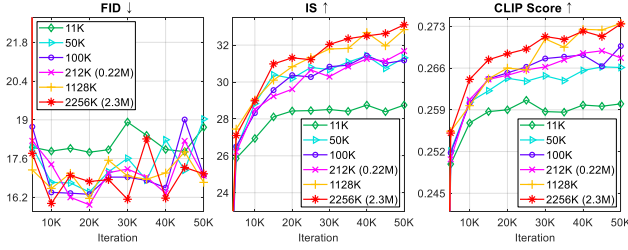


Figure 11. **Impact of training data volume.** Results of BK-SDM-Small on MS-COCO 30K.

the models retrained with a batch size of 64, the baselines without KD fail to generate the subjects or cannot maintain the identity details. See Sec. E for further results.

Image-to-image translation. Fig. 13 presents the text-guided stylization results with SDEdit [38]. Our model, resembling the ability of the original SDM, faithfully produces images given style-specified prompts and content pictures. See Sec. F for additional results.

Deployment on edge devices. We deploy our models trained with 2.3M pairs and compare them against the original SDM under the same setup on edge devices (20 denoising steps on NVIDIA Jetson AGX Orin 32GB and 10 steps on iPhone 14). Our models produce a 512×512 image within 4 seconds (see Tab. 7), while maintaining acceptable image quality (Fig. 1(d) and Sec. G).

Another LDM. SDMs are derived from LDMs [55], which share a similar U-Net design across many tasks. To validate the generality of our work, the same approach of BK-SDM-Small is applied to compress an LDM for unconditional generation on CelebA-HQ [54]. Fig. 14 shows the efficacy of our architecture and distillation retraining.

6. Conclusion

We uncover the potential of architectural compression for general-purpose text-to-image synthesis with a renowned model, Stable Diffusion. Our block-removed lightweight models are effective for zero-shot generation, achieving competitive results against large-scale baselines. Distillation is a key of our method, leading to powerful retraining even

Backbone {Param}	DINO↑	CLIP-I↑	CLIP-T↑	FT (Time, Mem) [†]
SDM-v1.4 [52] {1.04B}	0.728	0.725	0.263	(882s, 23.0GB)
BK-SDM-Base {0.76B}	0.723	0.717	0.260	(623s, 18.7GB)
BK-SDM-Small {0.66B}	0.720	0.705	0.259	(604s, 17.2GB)
BK-SDM-Tiny {0.50B}	0.715	0.693	0.261	(560s, 13.1GB)
Base (Batch 64) {0.76B}	0.718	0.708	0.262	(623s, 18.7GB)
- No KD & Random Init.	0.594	0.465	0.191	(623s, 18.7GB)
- No KD & Teacher Init.	0.716	0.669	0.258	(623s, 18.7GB)

[†]: Per-subject FT time and GPU memory for 800 iterations with a batch size of 1 on NVIDIA RTX 3090.

Table 6. **Personalized generation with finetuning over different backbones.** Our compact models can preserve subject fidelity (DINO and CLIP-I) and prompt fidelity (CLIP-T) of the original SDM with reduced finetuning (FT) costs and fewer parameters.

Device	SDM-v1	Base [Ours]	Small [Ours]	Tiny [Ours]
AGX Orin 32GB	4.9s [53]	3.4s (-31%)	3.2s (-35%)	2.8s (-43%)
iPhone 14	5.6s [52]	4.0s (-29%)	3.9s (-29%)	3.9s (-29%)

Table 7. **Inference speedup on edge devices.**



Figure 12. **Visual results of personalized generation.** Each subject is marked as “a [identifier] [class noun]” (e.g., “a [V] dog”).

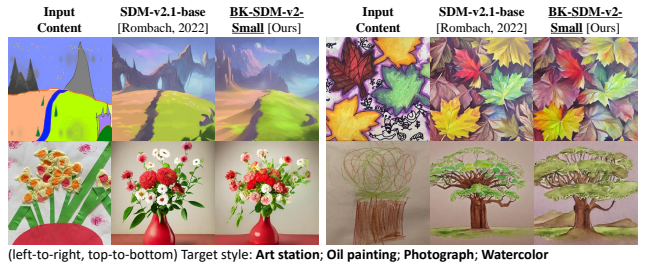


Figure 13. **Text-guided image-to-image translation.**



Figure 14. **Lightweight LDM for face generation.** The LDM (308M parameters; 410K training iterations) [54, 55] is compressed with the BK-SDM-Small approach (187M params; 30K iters).

under very constrained resources. Our work is orthogonal to previous works for efficient diffusion models, e.g., enabling fewer sampling steps, and can be readily combined with them. We hope our study can facilitate future research on structural compression of large diffusion models.

References

- [1] Stable diffusion web ui. <https://github.com/AUTOMATIC1111/stable-diffusion-webui>. 7, 9
- [2] Andreas Blattmann, Robin Rombach, Huan Ling, Tim Dockhorn, Seung Wook Kim, Sanja Fidler, and Karsten Kreis. Align your latents: High-resolution video synthesis with latent diffusion models. In *CVPR*, 2023. 1, 2
- [3] Tim Brooks, Aleksander Holynski, and Alexei A Efros. Instructpix2pix: Learning to follow image editing instructions. In *CVPR*, 2023. 1, 2
- [4] Mathilde Caron, Hugo Touvron, Ishan Misra, Hervé Jégou, Julien Mairal, Piotr Bojanowski, and Armand Joulin. Emerging properties in self-supervised vision transformers. In *ICCV*, 2021. 4
- [5] Yu-Hui Chen, Raman Sarokin, Juhyun Lee, Jiuqiang Tang, Chuo-Ling Chang, Andrei Kulik, and Matthias Grundmann. Speed is all you need: On-device acceleration of large diffusion models via gpu-aware optimizations. In *CVPR Workshop*, 2023. 1, 2
- [6] Jacob Devlin, Ming-Wei Chang, Kenton Lee, and Kristina Toutanova. Bert: Pre-training of deep bidirectional transformers for language understanding. In *NAACL*, 2019. 2
- [7] Prafulla Dhariwal and Alexander Nichol. Diffusion models beat gans on image synthesis. In *NeurIPS*, 2021. 1, 2
- [8] Ming Ding, Zhuoyi Yang, Wenyi Hong, Wendi Zheng, Chang Zhou, Da Yin, Junyang Lin, Xu Zou, Zhou Shao, Hongxia Yang, et al. Cogview: Mastering text-to-image generation via transformers. In *NeurIPS*, 2021. 2, 5
- [9] Ming Ding, Wendi Zheng, Wenyi Hong, and Jie Tang. Cogview2: Faster and better text-to-image generation via hierarchical transformers. In *NeurIPS*, 2022. 2, 5, 6, 4
- [10] Patrick Esser, Robin Rombach, and Bjorn Ommer. Taming transformers for high-resolution image synthesis. In *CVPR*, 2021. 1
- [11] Gongfan Fang, Xinyin Ma, Mingli Song, Michael Bi Mi, and Xinchao Wang. Depgraph: Towards any structural pruning. In *CVPR*, 2023. 2
- [12] Gongfan Fang, Xinyin Ma, and Xinchao Wang. Structural pruning for diffusion models. In *NeurIPS*, 2023. 2
- [13] Oran Gafni, Adam Polyak, Oron Ashual, Shelly Sheynin, Devi Parikh, and Yaniv Taigman. Make-a-scene: Scene-based text-to-image generation with human priors. In *ECCV*, 2022. 5
- [14] Zhiwei Hao, Jianyuan Guo, Ding Jia, Kai Han, Yehui Tang, Chao Zhang, Han Hu, and Yunhe Wang. Learning efficient vision transformers via fine-grained manifold distillation. In *NeurIPS*, 2022. 2
- [15] Kaiming He, Xiangyu Zhang, Shaoqing Ren, and Jian Sun. Deep residual learning for image recognition. In *CVPR*, 2016. 3
- [16] Byeongho Heo, Jeessoo Kim, Sangdoo Yun, Hyojin Park, Nojun Kwak, and Jin Young Choi. A comprehensive overhaul of feature distillation. In *ICCV*, 2019. 2, 4
- [17] Jack Hessel, Ari Holtzman, Maxwell Forbes, Ronan Le Bras, and Yejin Choi. CLIPScore: A reference-free evaluation metric for image captioning. In *EMNLP*, 2021. 4
- [18] Martin Heusel, Hubert Ramsauer, Thomas Unterthiner, Bernhard Nessler, and Sepp Hochreiter. Gans trained by a two time-scale update rule converge to a local nash equilibrium. In *NeurIPS*, 2017. 4
- [19] Geoffrey Hinton, Oriol Vinyals, and Jeff Dean. Distilling the knowledge in a neural network. In *NeurIPS Workshop*, 2014. 2, 4
- [20] Jonathan Ho and Tim Salimans. Classifier-free diffusion guidance. In *NeurIPS Workshop*, 2021. 1, 5, 7, 12
- [21] Jonathan Ho, Ajay Jain, and Pieter Abbeel. Denoising diffusion probabilistic models. In *NeurIPS*, 2020. 2, 4, 12
- [22] Jilei Hou and Ziad Asghar. World’s first on-device demonstration of stable diffusion on an android phone. <https://www.qualcomm.com/news>, 2023. 1, 2
- [23] Andrew Jaegle, Felix Gimeno, Andy Brock, Oriol Vinyals, Andrew Zisserman, and Joao Carreira. Perceiver: General perception with iterative attention. In *ICML*, 2021. 3
- [24] Xiaoqi Jiao, Yichun Yin, Lifeng Shang, Xin Jiang, Xiao Chen, Linlin Li, Fang Wang, and Qun Liu. Tinybert: Distilling bert for natural language understanding. In *Findings of EMNLP*, 2020. 2
- [25] Minguk Kang, Jun-Yan Zhu, Richard Zhang, Jaesik Park, Eli Shechtman, Sylvain Paris, and Taesung Park. Scaling up gans for text-to-image synthesis. In *CVPR*, 2023. 5
- [26] Tero Karras, Miika Aittala, Timo Aila, and Samuli Laine. Elucidating the design space of diffusion-based generative models. In *NeurIPS*, 2022. 7
- [27] Bo-Kyeong Kim, Shinkook Choi, and Hanchoul Park. Cut inner layers: A structured pruning strategy for efficient u-net gans. In *ICML Workshop*, 2022. 3, 4
- [28] Benjamin Lefaudeux, Francisco Massa, Diana Liskovich, Wenhan Xiong, Vittorio Caggiano, Sean Naren, Min Xu, Jieru Hu, Marta Tintore, Susan Zhang, Patrick Labatut, and Daniel Haziza. xformers: A modular and hackable transformer modelling library. <https://github.com/facebookresearch/xformers>, 2022. 7
- [29] Muyang Li, Ji Lin, Yaoyao Ding, Zhijian Liu, Jun-Yan Zhu, and Song Han. Gan compression: Efficient architectures for interactive conditional gans. In *CVPR*, 2020. 2
- [30] Xiuyu Li, Yijiang Liu, Long Lian, Huanrui Yang, Zhen Dong, Daniel Kang, Shanghang Zhang, and Kurt Keutzer. Q-diffusion: Quantizing diffusion models. In *ICCV*, 2023. 1, 2
- [31] Yanyu Li, Huan Wang, Qing Jin, Ju Hu, Pavlo Chemerys, Yun Fu, Yanzhi Wang, Sergey Tulyakov, and Jian Ren. Snapfusion: Text-to-image diffusion model on mobile devices within two seconds. In *NeurIPS*, 2023. 2, 5
- [32] Tsung-Yi Lin, Michael Maire, Serge Belongie, James Hays, Pietro Perona, Deva Ramanan, Piotr Dollár, and C Lawrence Zitnick. Microsoft coco: Common objects in context. In *ECCV*, 2014. 4
- [33] Luping Liu, Yi Ren, Zhijie Lin, and Zhou Zhao. Pseudo numerical methods for diffusion models on manifolds. In *ICLR*, 2022. 1, 12
- [34] Cheng Lu, Yuhao Zhou, Fan Bao, Jianfei Chen, Chongxuan Li, and Jun Zhu. Dpm-solver: A fast ode solver for diffusion probabilistic model sampling in around 10 steps. In *NeurIPS*, 2022. 2, 7, 12

- [35] Cheng Lu, Yuhao Zhou, Fan Bao, Jianfei Chen, Chongxuan Li, and Jun Zhu. Dpm-solver++: Fast solver for guided sampling of diffusion probabilistic models. *arXiv preprint arXiv:2211.01095*, 2022. 2, 7, 12
- [36] Sourab Mangrulkar, Sylvain Gugger, Lysandre Debut, Younes Belkada, and Sayak Paul. Peft: State-of-the-art parameter-efficient fine-tuning methods. <https://github.com/huggingface/peft>, 2022. 5, 12
- [37] Chenlin Meng, Ruiqi Gao, Diederik P Kingma, Stefano Ermon, Jonathan Ho, and Tim Salimans. On distillation of guided diffusion models. In *NeurIPS Workshop*, 2022. 1, 2
- [38] Chenlin Meng, Yutong He, Yang Song, Jiaming Song, Jiajun Wu, Jun-Yan Zhu, and Stefano Ermon. Sedit: Guided image synthesis and editing with stochastic differential equations. In *ICLR*, 2022. 2, 8, 12
- [39] Chenlin Meng, Ruiqi Gao, Diederik P Kingma, Stefano Ermon, Jonathan Ho, and Tim Salimans. On distillation of guided diffusion models. In *CVPR*, 2023. 1, 2, 4
- [40] Sangwoo Mo, Minsu Cho, and Jinwoo Shin. Freeze the discriminator: a simple baseline for fine-tuning gans. In *CVPR Workshop*, 2020. 5
- [41] Chaitanya Murti, Tanay Narshana, and Chiranjib Bhattacharyya. TVSPRune - pruning non-discriminative filters via total variation separability of intermediate representations without fine tuning. In *ICLR*, 2023. 2
- [42] Alex Nichol, Prafulla Dhariwal, Aditya Ramesh, Pranav Shyam, Pamela Mishkin, Bob McGrew, Ilya Sutskever, and Mark Chen. Glide: Towards photorealistic image generation and editing with text-guided diffusion models. In *ICML*, 2022. 2, 5, 6
- [43] Atila Orhon, Michael Siracusa, and Aseem Wadhwa. Stable diffusion with core ml on apple silicon, 2022. 7
- [44] Wonpyo Park, Dongju Kim, Yan Lu, and Minsu Cho. Relational knowledge distillation. In *CVPR*, 2019. 2
- [45] Pablo Pernias, Dominic Rampas, Mats L. Richter, Christopher J. Pal, and Marc Aubreville. Wuerstchen: An efficient architecture for large-scale text-to-image diffusion models. *arXiv preprint arXiv:2306.00637*, 2023. 2, 5, 6
- [46] Justin Pinkney. Small stable diffusion. <https://huggingface.co/OFA-Sys/small-stable-diffusion-v0>, 2023. 5
- [47] Alec Radford, Jeffrey Wu, Rewon Child, David Luan, Dario Amodei, Ilya Sutskever, et al. Language models are unsupervised multitask learners. *OpenAI blog*, 2019. 2
- [48] Alec Radford, Jong Wook Kim, Chris Hallacy, Aditya Ramesh, Gabriel Goh, Sandhini Agarwal, Girish Sastry, Amanda Askell, Pamela Mishkin, Jack Clark, et al. Learning transferable visual models from natural language supervision. In *ICML*, 2021. 1, 2, 4
- [49] Aditya Ramesh, Mikhail Pavlov, Gabriel Goh, Scott Gray, Chelsea Voss, Alec Radford, Mark Chen, and Ilya Sutskever. Zero-shot text-to-image generation. In *ICML*, 2021. 2, 4, 5
- [50] Aditya Ramesh, Prafulla Dhariwal, Alex Nichol, Casey Chu, and Mark Chen. Hierarchical text-conditional image generation with clip latents. *arXiv preprint arXiv:2204.06125*, 2022. 2, 5
- [51] Yuxi Ren, Jie Wu, Xuefeng Xiao, and Jianchao Yang. Online multi-granularity distillation for gan compression. In *ICCV*, 2021. 2, 4
- [52] Robin Rombach and Patrick Esser. Stable diffusion v1-4. <https://huggingface.co/CompVis/stable-diffusion-v1-4>, 2022. 1, 2, 3, 4, 5, 7, 8
- [53] Robin Rombach and Patrick Esser. Stable diffusion v1-5. <https://huggingface.co/runwayml/stable-diffusion-v1-5>, 2022. 2, 8, 7
- [54] Robin Rombach, Andreas Blattmann, Dominik Lorenz, Patrick Esser, and Björn Ommer. Ldm on celeba-hq. <https://huggingface.co/CompVis/ldm-celebahq-256>, 2022. 8
- [55] Robin Rombach, Andreas Blattmann, Dominik Lorenz, Patrick Esser, and Björn Ommer. High-resolution image synthesis with latent diffusion models. In *CVPR*, 2022. 1, 2, 4, 5, 8, 7
- [56] Robin Rombach, Patrick Esser, and David Ha. Stable diffusion v2-1-base. <https://huggingface.co/stabilityai/stable-diffusion-2-1-base>, 2022. 2, 3, 4, 5
- [57] Adriana Romero, Nicolas Ballas, Samira Ebrahimi Kahou, Antoine Chassang, Carlo Gatta, and Yoshua Bengio. Fitnets: Hints for thin deep nets. In *ICLR*, 2015. 2, 4
- [58] Olaf Ronneberger, Philipp Fischer, and Thomas Brox. U-net: Convolutional networks for biomedical image segmentation. In *MICCAI*, 2015. 1, 3
- [59] Nataniel Ruiz, Yuanzhen Li, Varun Jampani, Yael Pritch, Michael Rubinstein, and Kfir Aberman. Dreambooth: Fine tuning text-to-image diffusion models for subject-driven generation. In *CVPR*, 2023. 2, 4, 7
- [60] Chitwan Saharia, William Chan, Saurabh Saxena, Lala Li, Jay Whang, Emily L Denton, Kamyar Ghasemipour, Raphael Gontijo Lopes, Burcu Karagol Ayan, Tim Salimans, et al. Photorealistic text-to-image diffusion models with deep language understanding. In *NeurIPS*, 2022. 2, 4, 5, 7, 12
- [61] Tim Salimans and Jonathan Ho. Progressive distillation for fast sampling of diffusion models. In *ICLR*, 2022. 2
- [62] Tim Salimans, Ian Goodfellow, Wojciech Zaremba, Vicki Cheung, Alec Radford, and Xi Chen. Improved techniques for training gans. In *NeurIPS*, 2016. 4
- [63] Victor Sanh, Lysandre Debut, Julien Chaumond, and Thomas Wolf. Distilbert, a distilled version of bert: smaller, faster, cheaper and lighter. In *NeurIPS Workshop*, 2019. 2, 3, 4
- [64] Christoph Schuhmann and Romain Beaumont. Laion-aesthetics. <https://laion.ai/blog/laion-aesthetics>, 2022. 2, 4
- [65] Christoph Schuhmann, Romain Beaumont, Richard Vencu, Cade Gordon, Ross Wightman, Mehdi Cherti, Theo Coombes, Aarush Katta, Clayton Mullis, Mitchell Wortsman, et al. Laion-5b: An open large-scale dataset for training next generation image-text models. In *NeurIPS Workshop*, 2022. 4
- [66] Segmind. Segmind-distill-sd. <https://github.com/segmind/distill-sd/tree/c1e97a70d141df09e6fe5cc7dbd66e0cbeae3eeb>, 2023. 2

- [67] Segmind. Ssd-1b. <https://github.com/segmind/SSD-1B/tree/d2ff723ea8ecf5dbd86f3aac0af1db30e88a2e2d>, 2023. 2
- [68] Haihao Shen, Penghui Cheng, Xinyu Ye, Wenhua Cheng, and Huma Abidi. Accelerate stable diffusion with intel neural compressor. <https://medium.com/intel-analytics-software>, 2022. 1, 2
- [69] Changyong Shu, Yifan Liu, Jianfei Gao, Zheng Yan, and Chunhua Shen. Channel-wise knowledge distillation for dense prediction. In *ICCV*, 2021. 4
- [70] Jiaming Song, Chenlin Meng, and Stefano Ermon. Denoising diffusion implicit models. In *ICLR*, 2021. 1, 2
- [71] Zhiqing Sun, Hongkun Yu, Xiaodan Song, Renjie Liu, Yiming Yang, and Denny Zhou. Mobilebert: a compact task-agnostic bert for resource-limited devices. In *ACL*, 2020. 2
- [72] Raphael Tang, Linqing Liu, Akshat Pandey, Zhiying Jiang, Gefei Yang, Karun Kumar, Pontus Stenetorp, Jimmy Lin, and Ferhan Ture. What the DAAM: Interpreting stable diffusion using cross attention. In *ACL*, 2023. 6
- [73] Ming Tao, Bing-Kun Bao, Hao Tang, and Changsheng Xu. Galip: Generative adversarial clips for text-to-image synthesis. In *CVPR*, 2023. 5, 6, 4
- [74] Hugo Touvron, Matthieu Cord, Matthijs Douze, Francisco Massa, Alexandre Sablayrolles, and Herve Jegou. Training data-efficient image transformers and distillation through attention. In *ICML*, 2021. 2
- [75] Aaron Van Den Oord, Oriol Vinyals, et al. Neural discrete representation learning. In *NeurIPS*, 2017. 1
- [76] Ashish Vaswani, Noam Shazeer, Niki Parmar, Jakob Uszkoreit, Llion Jones, Aidan N Gomez, Łukasz Kaiser, and Illia Polosukhin. Attention is all you need. In *NeurIPS*, 2017. 3
- [77] Patrick von Platen, Suraj Patil, Anton Lozhkov, Pedro Cuenca, Nathan Lambert, Kashif Rasul, Mishig Davaadorj, and Thomas Wolf. Diffusers: State-of-the-art diffusion models. <https://github.com/huggingface/diffusers>, 2022. 5, 12
- [78] Haochen Wang, Xiaodan Du, Jiahao Li, Raymond A Yeh, and Greg Shakhnarovich. Score jacobian chaining: Lifting pretrained 2d diffusion models for 3d generation. In *CVPR*, 2023. 1, 2
- [79] Lu Yu and Wei Xiang. X-pruner: explainable pruning for vision transformers. In *CVPR*, 2023. 2
- [80] Sergey Zagoruyko and Nikos Komodakis. Paying more attention to attention: Improving the performance of convolutional neural networks via attention transfer. In *ICLR*, 2017. 2
- [81] Lvmin Zhang and Maneesh Agrawala. Adding conditional control to text-to-image diffusion models. In *ICCV*, 2023. 1
- [82] Linfeng Zhang, Xin Chen, Xiaobing Tu, Pengfei Wan, Ning Xu, and Kaisheng Ma. Wavelet knowledge distillation: Towards efficient image-to-image translation. In *CVPR*, 2022. 2
- [83] Qinsheng Zhang and Yongxin Chen. Fast sampling of diffusion models with exponential integrator. In *ICLR*, 2023. 2
- [84] Yufan Zhou, Ruiyi Zhang, Changyou Chen, Chunyuan Li, Chris Tensmeyer, Tong Yu, Jiuxiang Gu, Jinhui Xu, and Tong Sun. Towards language-free training for text-to-image generation. In *CVPR*, 2022. 5, 6, 4
- [85] Ligeng Zhu. Thop: Pytorch-opcounter. <https://github.com/Lyken17/pytorch-OpCounter>, 2018. 2

BK-SDM: A Lightweight, Fast, and Cheap Version of Stable Diffusion

Appendix

A. U-Net architecture and distillation retraining of BK-SDM

Figs. 15 and 16 depict the U-Net architectures and distillation process, respectively. Our approach is directly applicable to all the SDM versions in v1 and v2 (i.e., v1.1/2/3/4/5, v2.0/1, and v2.0/1-base), which share the same U-Net block configuration. See Fig. 17 for the block details.

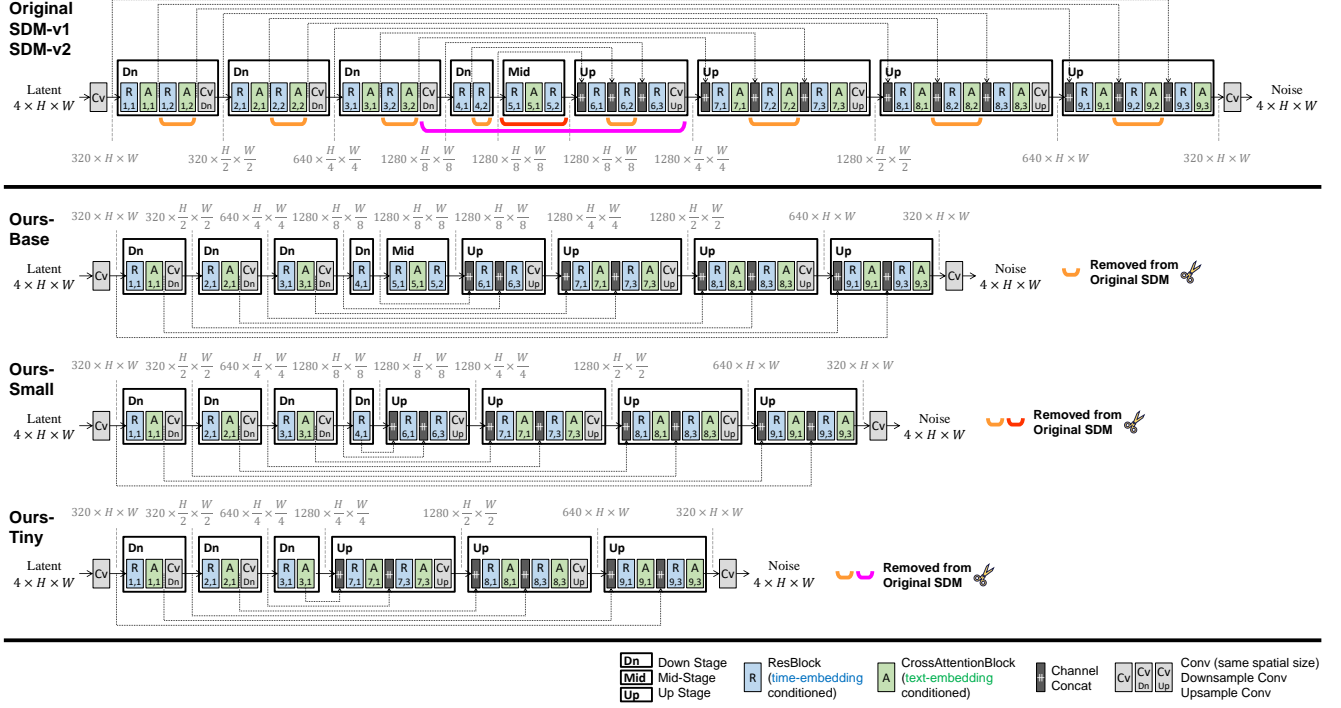


Figure 15. U-Net architectures of SDM-v1, SDM-v2, and BK-SDMs.

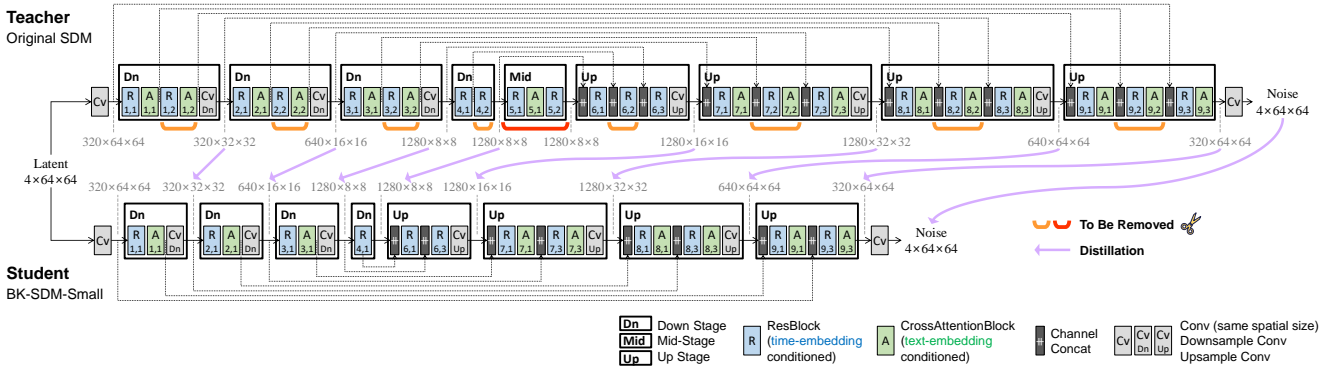


Figure 16. Distillation retraining process. The compact U-Net student is built by eliminating several residual and attention blocks from the original U-Net teacher. Through the feature and output distillation from the teacher, the student can be trained effectively yet rapidly. The default latent resolution for SDM-v1 and v2-base is $H = W = 64$ in Fig. 15, resulting in 512×512 generated images.

Fig. 17 shows the details of architectural blocks. Each residual block (ResBlock) contains two 3-by-3 convolutional layers and is conditioned on the time-step embedding. Each attention block (AttnBlock) contains a self-attention module, a cross-attention module, and a feed-forward network. The text embedding is merged via the cross-attention module. Within the attention block, the feature spatial dimensions h and w are flattened into a sequence length of hw . The number of channels c is considered as an embedding size, processed with attention heads. The number of groups for the group normalization is set to 32. The differences between SDM-v1 and SDM-v2 include the number of attention heads (8 for all the stages of SDM-v1 and [5, 10, 20, 20] for different stages of SDM-v2) and the text embedding dimensions (77×768 for SDM-v1 and 77×1024 for SDM-v2).

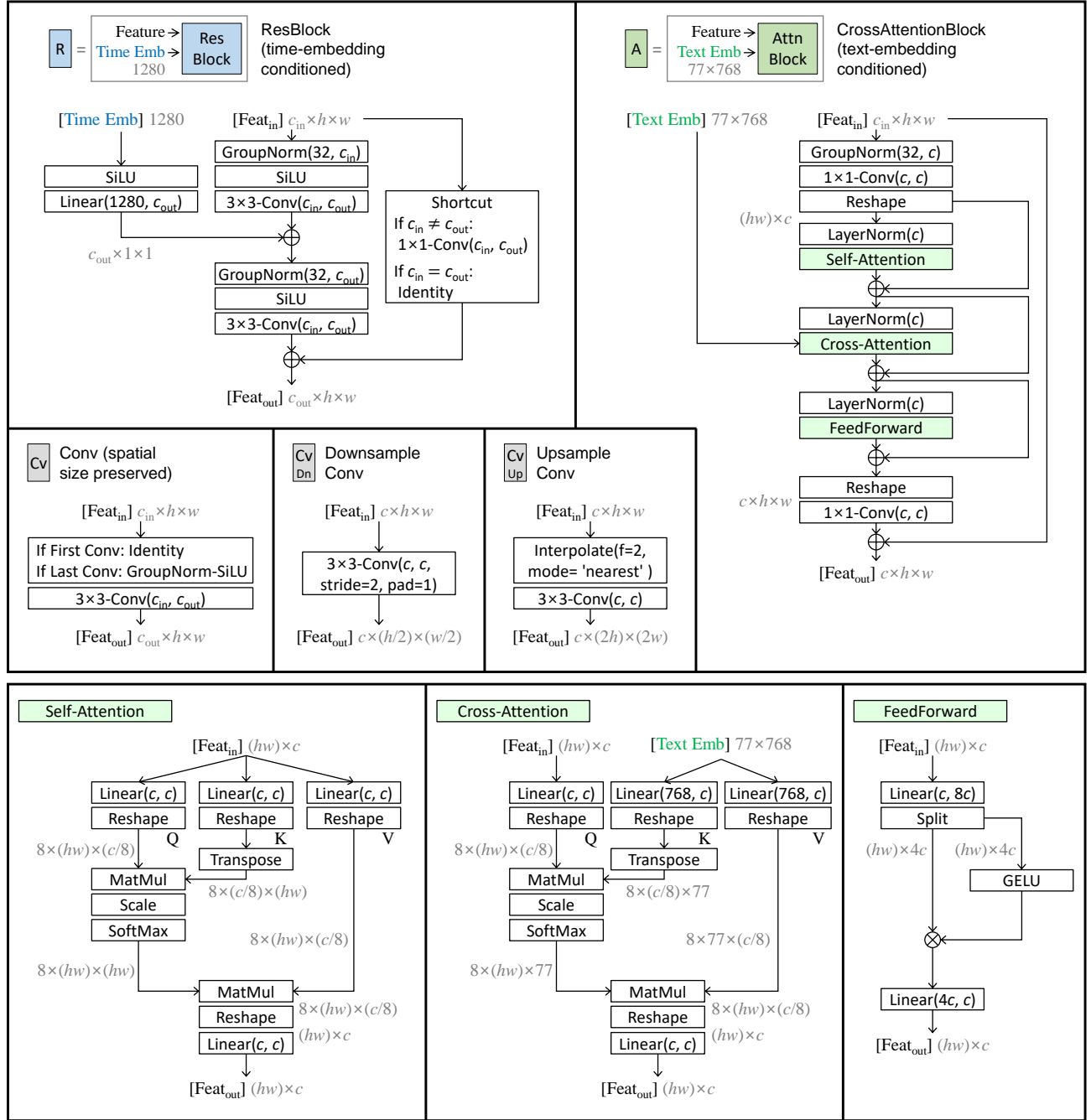


Figure 17. Block components in the U-Net.

B. Impact of the mid-stage removal

Removing the entire mid-stage from the original U-Net does not noticeably degrade the generation quality for many text prompts while effectively reducing the number of parameters. See Fig. 18 and Tab. 8.

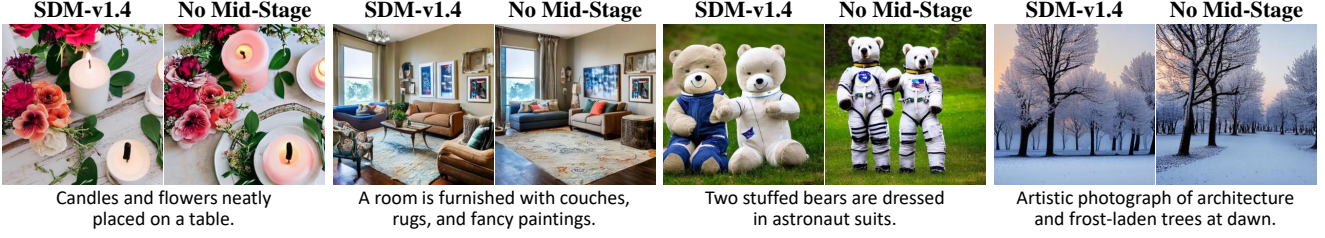


Figure 18. Visual results of the mid-stage removed U-Net from SDM-v1.4 [52]. Retraining is not performed.

Model	Performance		# Parameters	
	FID ↓	IS ↑	U-Net	Whole
SDM-v1.4 [52]	13.05	36.76	859.5M	1032.1M
Mid-Stage Removal	15.60	32.33	762.5M (-11.3%)	935.1M (-9.4%)

Table 8. Minor impact of eliminating the mid-stage on zero-shot MS-COCO 256×256 30K. Retraining is not performed.

C. Block-level pruning sensitivity analysis

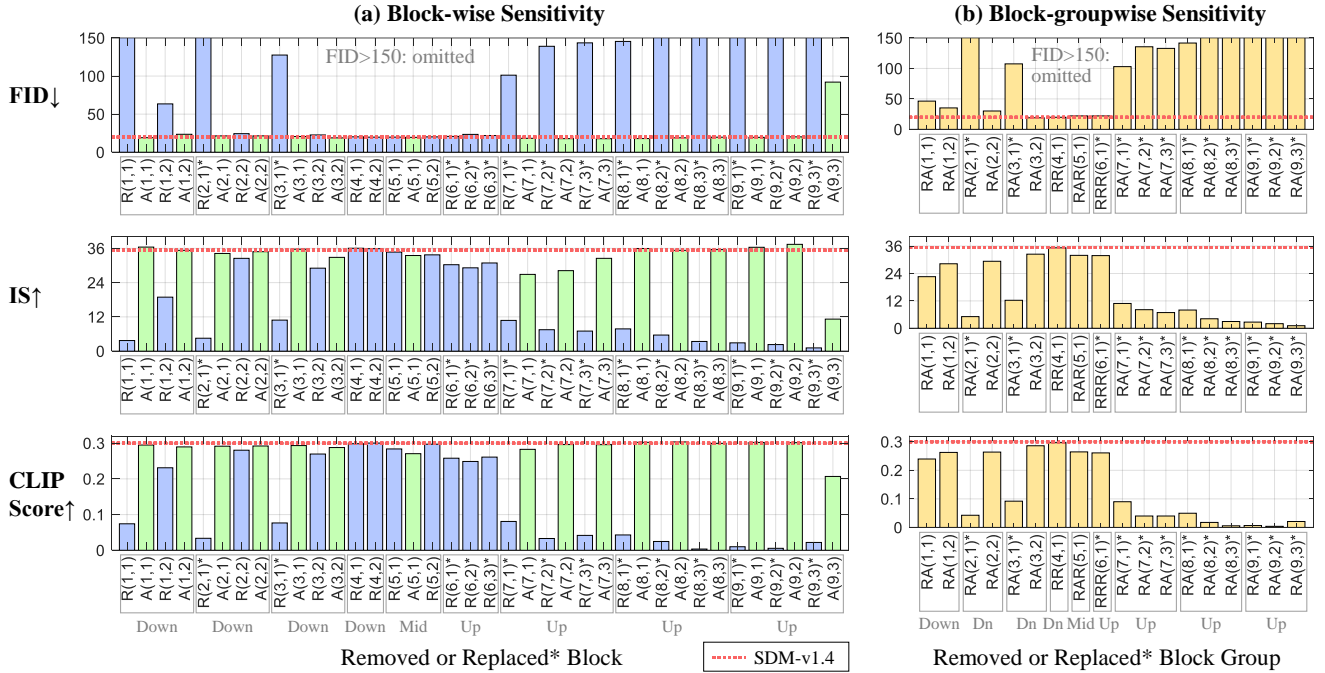


Figure 19. Analyzing the importance of (a) each block and (b) each group of paired/triplet blocks in SDM-v1.4. Evaluation on MS-COCO 512×512 5K. The block notations match Fig. 15. Whenever possible (i.e., with the same dimensions of input and output), we remove each block to examine its effect on generation performance. For blocks with different channel dimensions of input and output, we replace them with channel interpolation modules (denoted by “*”) to mimic the removal while retaining the information. The results are aligned with our architectural choices (e.g., removal of innermost stages and the second R-A pairs in down stages).

D. Comparison with existing studies








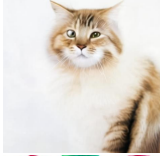



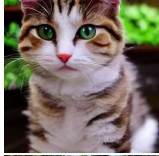
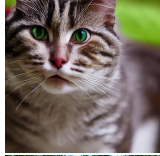
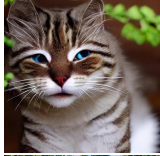
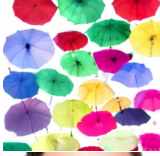



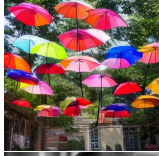
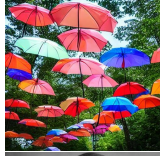

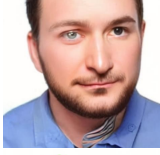
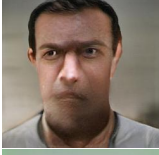



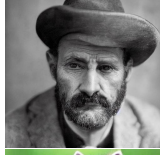
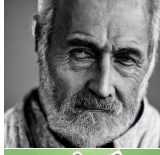













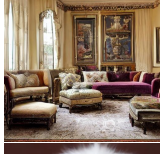




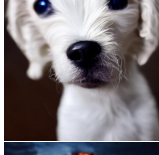
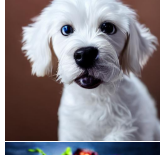




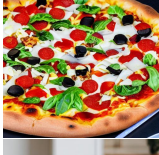










	CogView2 (Ding, 2022)	LAFITE (Zhou, 2022)	GALIP-CC12M (Tao, 2023)	SDM-v1.4 (Rombach, 2022)	BK-SDM-Base (Ours)	BK-SDM-Small (Ours)	BK-SDM-Tiny (Ours)
A bowl that has vegetables inside of it.							
A brown and white cat staring off with pretty green eyes.							
There are many decorative umbrellas hanging up.							
A man staring ahead at the camera with a neutral expression.							
A toy raccoon standing on a pile of broccoli.							
An ornate living room set sits in a large house.							
A small white dog looking into a camera.							
A very close up picture of a pizza with several toppings.							
Small green vase on counter with floral arrangement.							

Figure 20. Zero-shot general-purpose T2I results. The results of previous studies [9, 73, 84] were obtained with their official codes and released models. We do not apply any CLIP-based reranking for SDM and our models.

E. Personalized generation



Figure 21. Results of personalized generation. Each subject is marked as “a [identifier] [class noun]” (e.g., “a [V] dog”). Similar to the original SDM, our compact models can synthesize the images of input subjects in different backgrounds while preserving their appearance.

F. Text-guided image-to-image translation

Input Content	SDM-v2.1-base (Rombach, 2022)	BK-SDM-v2- Base (Ours)	BK-SDM-v2- Small (Ours)	BK-SDM-v2- Tiny (Ours)	SDM-v1.4 (Rombach, 2022)	BK-SDM- Tiny (Ours)	
							Man+ Anim
							Man+ ArtStation
							Woman+ Oil
							Woman+ Photo
							Watercolor
							Van Gogh
							Oil
							ArtStation
							Photo

Figure 22. Results of text-guided image-to-image translation. Our small models effectively stylize input images.

G. Deployment on edge devices

Our models are tested on NVIDIA Jetson AGX Orin 32GB, benchmarked against SDM-v1.5 [53, 55] under the same default setting of Stable Diffusion WebUI [1]. For the inference, 20 denoising steps, DPM++ 2M Karras sampling [26, 35], and xFormers-optimized attention [28] are used to synthesize 512×512 images. BK-SDM demonstrates quicker generation at 3.4 seconds, compared to the 4.9 seconds of SDM-v1.5 (see Figs. 23 and 26 with BK-SDM-Base trained on 2.3M pairs).

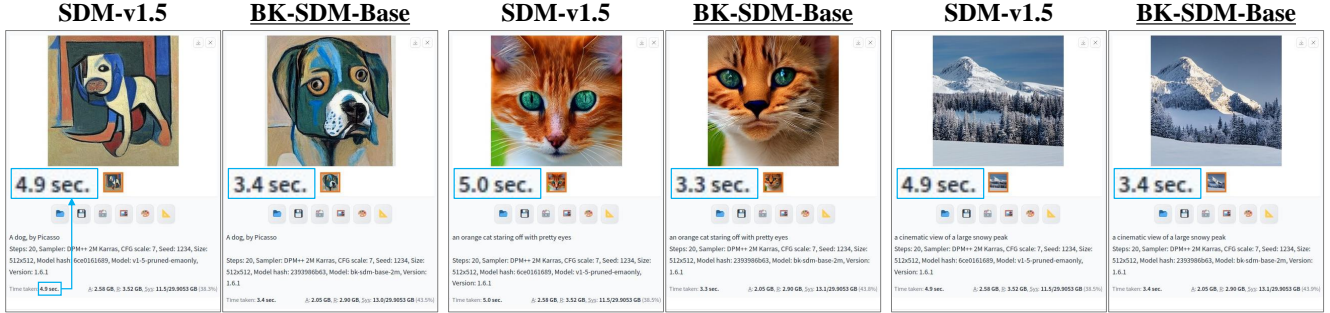


Figure 23. Deployment on NVIDIA Jetson AGX Orin 32GB.

We also deploy our models on iPhone 14 with post-training palettization [43] and compare them against the original SDM-v1.4 [52, 55] converted with the identical setup. With 10 denoising steps and DPM-Solver [34, 35], 512×512 images are generated from given prompts. The inference takes 3.9 seconds using BK-SDM, which is faster than 5.6 seconds using SDM-v1.4, while maintaining acceptable image quality (see Fig. 24 with BK-SDM-Small trained on 2.3M pairs).

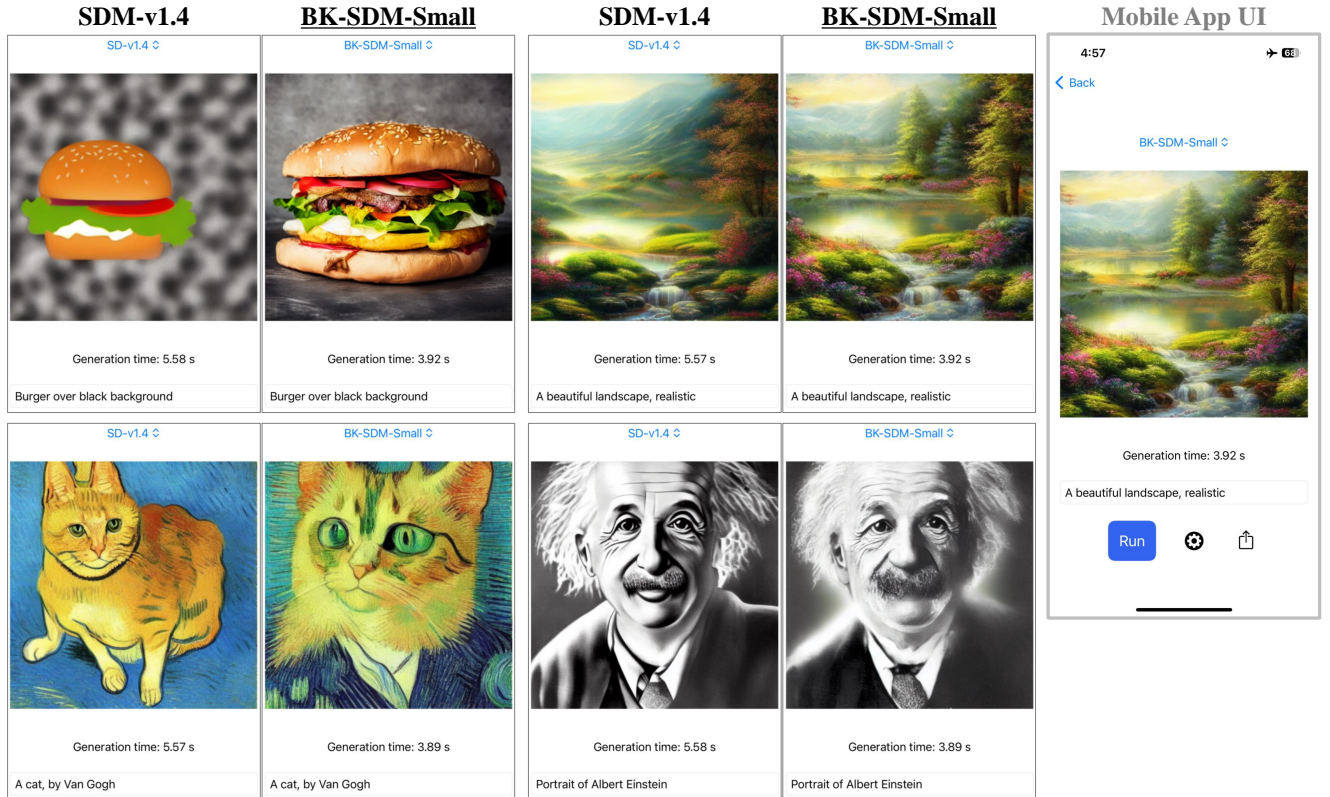
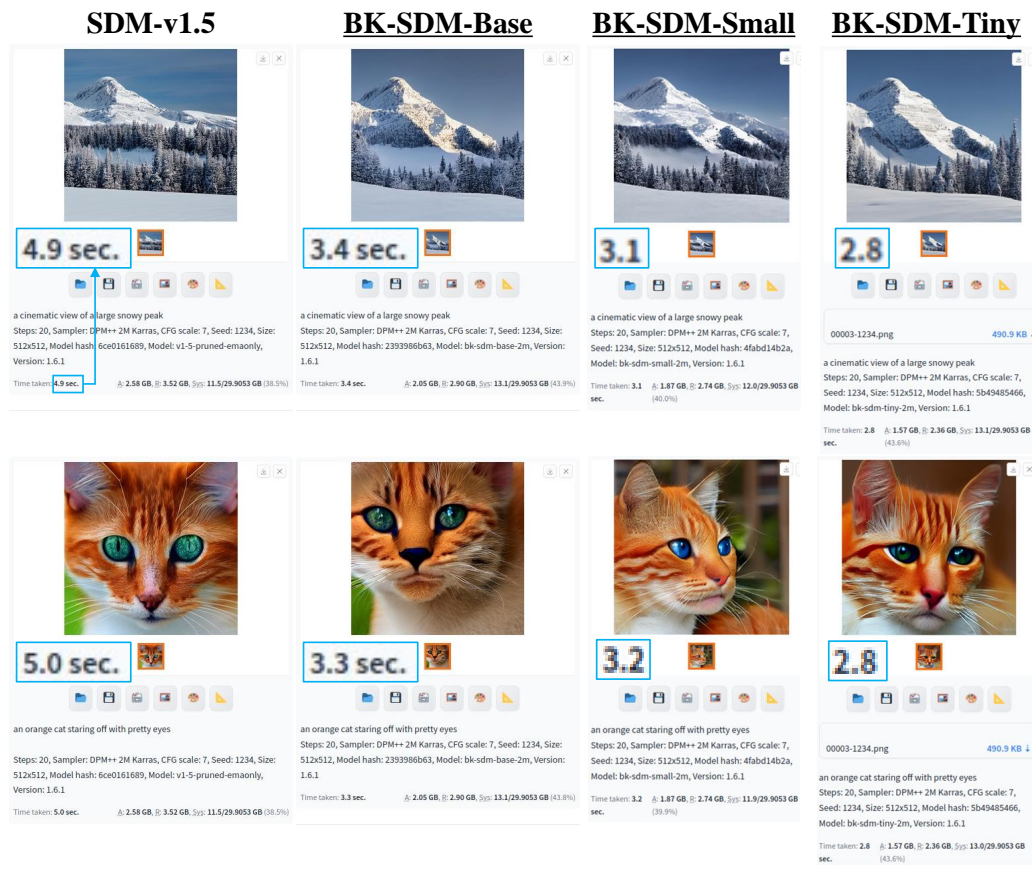


Figure 24. Deployment on iPhone 14.

Additional results using different models can be found in Fig. 25.

Jetson AGX
Orin 32GB



iPhone 14

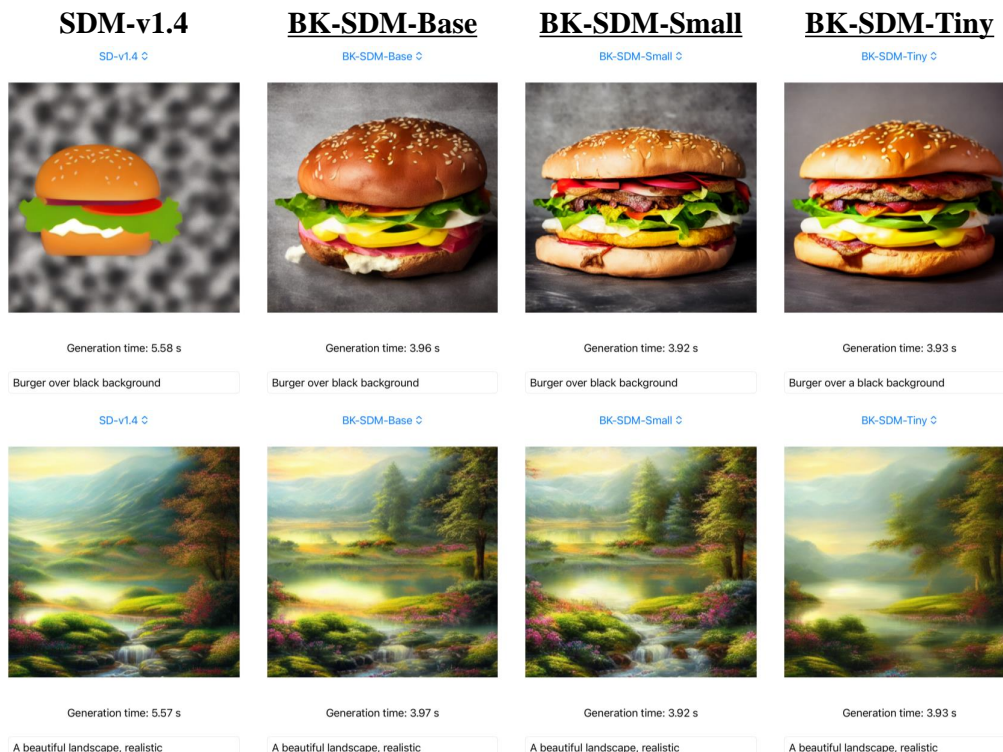


Figure 25. Additional examples from deployment on edge devices.

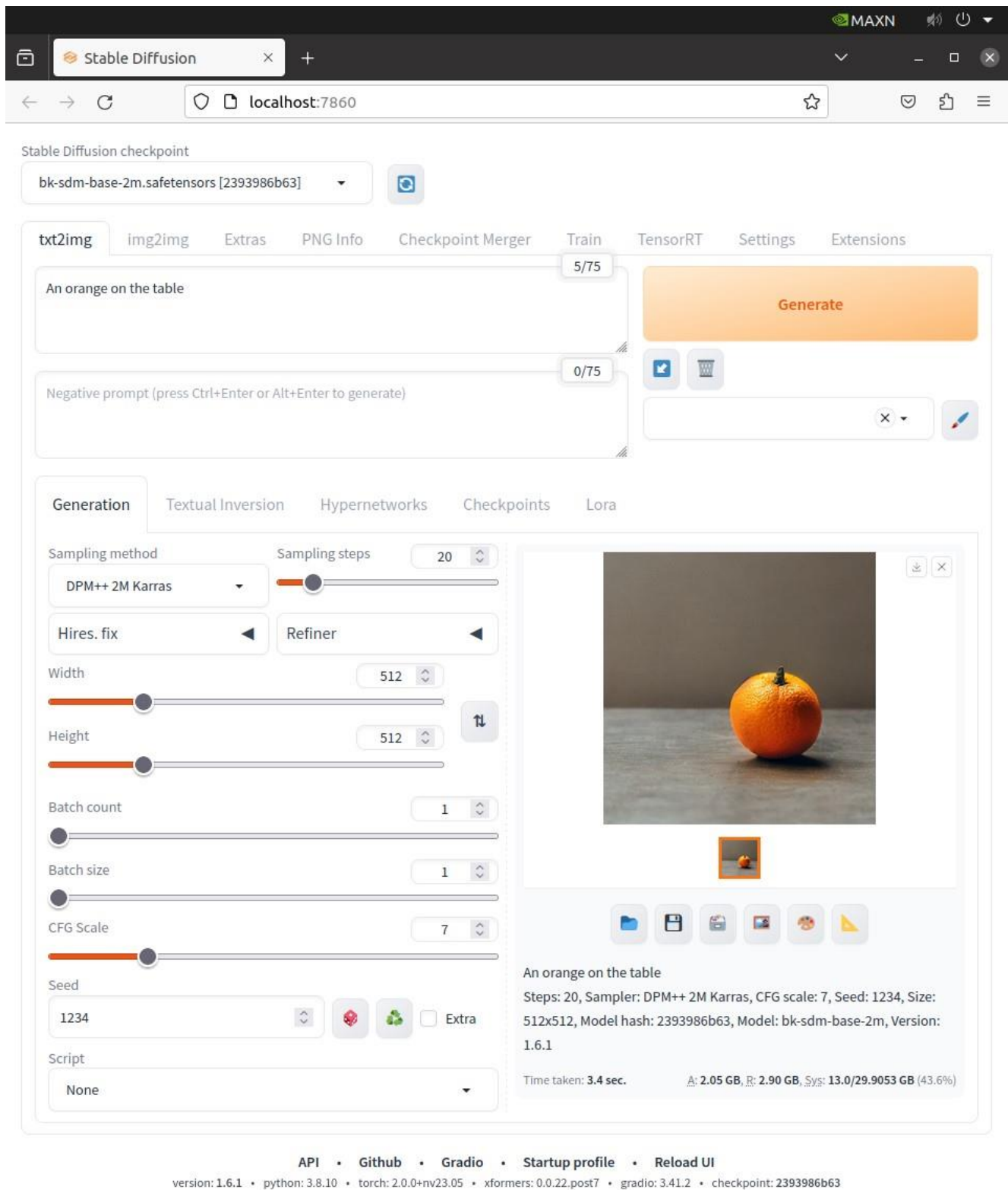


Figure 26. Stable Diffusion WebUI [1] used in the deployment on AGX Orin.

H. Impact of training data volume

Fig. 27 illustrates how varying data sizes affects the training of BK-SDM-Small. Fig. 28 presents additional visual outputs of the following models: BK-SDM-{Base, Small, Tiny} trained on 212K (i.e., 0.22M) pairs and BK-SDM-{Base-2M, Small-2M, Tiny-2M} trained on 2256K (2.3M) pairs.

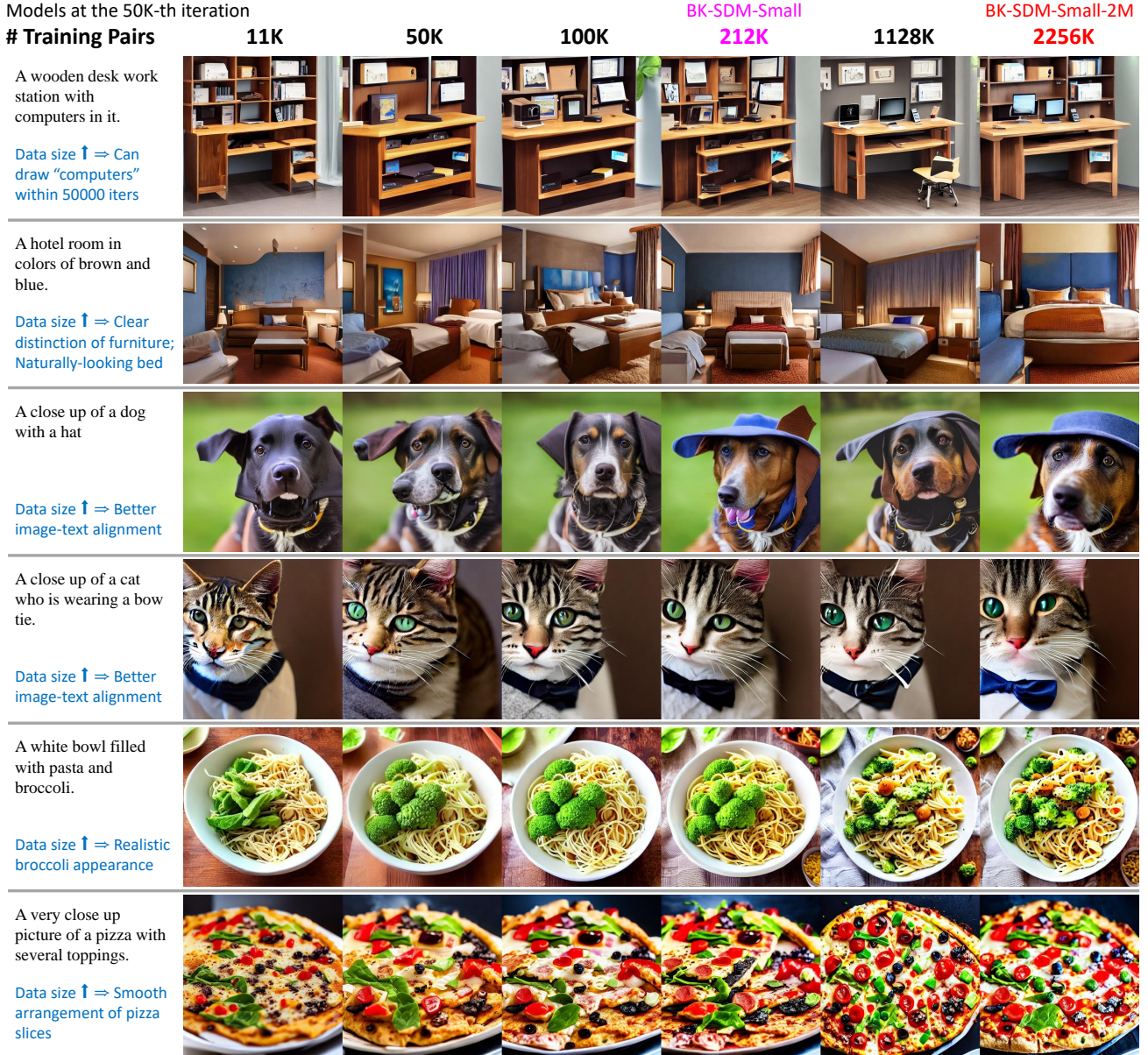


Figure 27. Varying data quantities in training BK-SDM-Small. As the amount of data increases, the visual outcomes improve, such as enhanced image-text matching and clearer differentiation between objects.

BK-SDM Type

A double bed in a hotel or motel setting.



A metal vase filled with yellow roses on top of a table.



A small tan and striped bird is sits on the branch of a red flowering bush.



A tray of food on the top of a table.



A boy wearing a tie and a white shirt.



The living room is all decorated for Christmas.



Figure 28. Results of BK-SDM- $\{\text{Base, Small, Tiny}\}$ trained on 0.22M pairs and $\{\text{Base-2M, Small-2M, Tiny-2M}\}$ trained on 2.3M pairs.

I. Implementation

We adjust the codes in Diffusers [77] for distillation retraining and PEFT [36] for per-subject finetuning, both of which adopt the training process of DDPM [21] in latent spaces.

Distillation retraining for general-purpose T2I. For augmentation, smaller edge of each image is resized to 512, and a center crop of size 512 is applied with random flip. We use a single NVIDIA A100 80G GPU for 50K-iteration retraining with the AdamW optimizer and a constant learning rate of $5e-5$. The number of steps for gradient accumulation is always set to 4. With a total batch size of 256 ($=4 \times 64$), it takes about 300 hours and 53GB GPU memory. Training smaller architectures results in 5~10% decrease in GPU memory usage.

DreamBooth finetuning. For augmentation, smaller edge of each image is resized to 512, and a random crop of size 512 is applied. We use a single NVIDIA GeForce RTX 3090 GPU to finetune each personalized model for 800 iterations with the AdamW optimizer and a constant learning rate of $1e-6$. We jointly finetune the text encoder as well as the U-Net. For each subject, 200 class images are generated by the original SDM. The weight of prior preservation loss is set to 1. With a batch size of 1, the original SDM requires 23GB GPU memory for finetuning, whereas BK-SDMs require 13~19GB memory.

Inference setup. Following the default setup, we use PNDM scheduler [33] for zero-shot T2I generation and DPM-Solver [34, 35] for DreamBooth results. For compute efficiency, we always opt for 25 denoising steps of the U-Net, unless specified. The classifier-free guidance scale [20, 60] is set to the default value of 7.5, except the analysis in Fig. 10.

Image-to-image translation. We use the SDEdit method [38] implemented in Diffusers [77], with the strength value of 0.8.

Distillation retraining for unconditional face generation. A similar approach to our T2I training is applied. For the 30K-iteration retraining, we use a batch size of 64 ($=4 \times 16$) and set the KD loss weights to 100.